

## Article

# Synthesis, Spectroscopic Characterization and Biological Studies of Mn(II), Cu(II), Ni(II), Co(II) and Zn(II) Complexes with New Schiff Base of 2-((Pyrazine-2-ylimino)methyl)phenol

Hanan B. Howsai<sup>1</sup>, Abeer A. Sharfalddin<sup>1</sup>, Magda H. Abdellattif<sup>2</sup>, Amal S. Basaleh<sup>1</sup>  
and Mostafa A. Hussien<sup>1,3,\*</sup> 

<sup>1</sup> Department of Chemistry, Faculty of Science, King Abdulaziz University, P.O. Box 80203, Jeddah 21589, Saudi Arabia; HHowsai0001@stu.kau.edu.sa (H.B.H.); sharfalddin.aa@gmail.com (A.A.S.); abasaleh@kau.edu.sa (A.S.B.)

<sup>2</sup> Chemistry Department, College of Sciences, Taif University, P.O. Box 11099, Taif 21944, Saudi Arabia; m.hasan@tu.edu.sa

<sup>3</sup> Department of Chemistry, Faculty of Science, Port Said University, Port Said 42521, Egypt

\* Correspondence: maabdulaal@kau.edu.sa



**Citation:** Howsai, H.B.; Sharfalddin, A.A.; Abdellattif, M.H.; Basaleh, A.S.; Hussien, M.A. Synthesis, Spectroscopic Characterization and Biological Studies of Mn(II), Cu(II), Ni(II), Co(II) and Zn(II) Complexes with New Schiff Base of 2-((Pyrazine-2-ylimino)methyl)phenol. *Appl. Sci.* **2021**, *11*, 9067. <https://doi.org/10.3390/app11199067>

Academic Editor: Susana Santos Braga

Received: 4 August 2021

Accepted: 7 September 2021

Published: 29 September 2021

**Publisher's Note:** MDPI stays neutral with regard to jurisdictional claims in published maps and institutional affiliations.



**Copyright:** © 2021 by the authors. Licensee MDPI, Basel, Switzerland. This article is an open access article distributed under the terms and conditions of the Creative Commons Attribution (CC BY) license (<https://creativecommons.org/licenses/by/4.0/>).

**Abstract:** In the search for novel anticancer complex, transition metal complexes of Schiff base derived from 2-aminopyrazine and salicylaldehyde were successfully synthesized and characterized based on elemental analyses, spectroscopic and thermal analysis. The IR spectra showed the ligand is a tridentate chelator with O, N and N atoms. donor sites in the Zn(II), Co(II), Ni(II), and Mn(II) complexes. Contrary, it behaved a bidentate chelator in the Cu complex by O and N. Molar ratio data revealed that the ligand to metal ratio was 1:2 for Co(II) Cu(II) and Zn(II) while it was 1:1 for Mn(II) and Ni(II) complexes. The obtained complexes have the formulae  $[M(L)_2]$  (where M = Co(II) and Zn(II)),  $[M(L)Cl(2H_2O)] \cdot H_2O$  (where M = Ni(II) and Mn(II)) were octahedral geometry. The computational studies were performed by DFT calculations to compare the optimized geometries with the experimental values. The interaction of these complexes with calf thymus DNA (CT-DNA) was investigated by UV-Vis spectroscopic technique. Molecular docking studies were against three protein cancer to investigate the binding ability of the new compounds. The anticancer activity was studied with different cell lines and the  $IC_{50}$  of the Cu(II) complex for (HOP-62) showed a practical result. The  $LD_{50}$  values of Zn(II) and Co(II) complexes showed that they are non-toxic at doses up to 370 mg/kg.

**Keywords:** transition metal complexes; Schiff base; DFT; molecular docking; DNA binding

## 1. Introduction

The importance of the heterocyclic compounds came from the diversity usage in industries, biological fields [1,2] and in analytical chemistry as analytical reagents for metal ion detection [3] or dyes synthesis, cosmetics, plastics and pharmaceutical products. Moreover, they play a practical role in the drug industry by designing and developing medicines and their wide applications [4]. One of the essential chemical structure classes is nitrogen heterocycles which are particularly well represented between natural products, biologically active structures, and medical-related compounds [3]. Among the most distinguished types, phenanthridine, indole, pyrazine, quinoline, and isoquinoline compounds which have gained significant interest in organic synthesis, medical chemistry, and materials science [5]. Schiff bases are an important class of organic compounds especially the ones synthesized from heterocyclic compounds, due to their chelating properties and ability to coordinate with a wide range of actinide, lanthanide and transition ions in various oxidation states using oxygen and nitrogen or other atoms to form stable complexes [6]. Several Schiff bases were prepared to contain nitrogen atoms with crucial biological activity such as antimicrobial, antioxidant, anticancer, anti-HIV activity, analgesic, anti-inflammatory [3,7].

It was reported when metal ions are introduced into the molecules of the compound it could improve their biological properties by decreasing their toxicity and enhancing their lipophilicity, absorbance, and stability [7]. Additionally, the presence of an imine (-C=N-) or azomethine (-HC=N-) group in Schiff bases contributes to linkage provides much flexibility in the design ligands for metal ion coordination [3,8]. Interestingly, most of the studies confirmed complexes of Schiff bases with transition metals are showed higher biological activities than their corresponding ligand [8]. Akmal S. Gaballa et al. synthesized Pt(II) complexes with Schiff bases derived from salicylaldehyde. The Schiff base ligand and its Pt(II) complexes have been tested in vitro to evaluate their antibacterial activity against eight types of bacteria. The activity data show that the Pt(II) complexes are more potent antimicrobials than the parent Schiff base ligands against one or more microorganisms [9]. Xueguang Ran et al. synthesized three salicylaldehyde derivatives Schiff base ligand and their Zn(II), Cu(II), and Co(II) complexes. These compounds were screened and evaluated by antibacterial and antifungal bioassay and showed that the metal complexes have more active than the free ligand. Among these complexes, the Cu(II) complex was the most effective compared to other complexes [10]. Another reported work presented eight vanadium complexes derived from Schiff bases and tested their inhibition toward human recombinant PTP1B by selected complexes, glucose consumption and cytotoxicity tests in adipocytes in 3T3-L1 cell line. All vanadium complexes were noncytotoxic and three complexes were found to be active in the inhibition of human recombinant PTP1B [11].

In this study, Schiff bases and their transition metal complexes Mn(II), Cu(II), Ni(II), Co(II), and Zn(II) were synthesized and characterized by various techniques. The interaction of Schiff bases and their transition metal complexes with biological targets were tested with CT-DNA. Molecular docking was used to simulate the binding of the investigated complexes with three types of cancer proteins. Finally, we tested the complexes in vitro activity against three cancer cell lines via (Ovar3), (M14), and (NSCLC).

## 2. Materials and Instruments

All starting materials and reagents were purchased from Alfa Aesar. The ACROS. Calf thymus (CT-DNA) and all solvents were purchased from Sigma-Aldrich. IR spectra were recorded in Bruker Alpha in the range of 400–4000  $\text{cm}^{-1}$ . UV-Vis spectra in the range of 200–800 nm were collected using a MultiSpec-1501 with a solution of  $10^{-3}$  M in DMSO at room temperature using matched 1.0 cm quartz cells. The  $^1\text{H}$  NMR spectra in DMSO- $d_6$  solution were recorded on Bruker Avance 600 MHz. Thermal analysis was carried out on a PerkinElmer TGA system until 1000 °C in the air with a heating rate of 10 °C/min. The solid sample EPR analysis was obtained using the continuous wave Bruker EMX PLUS spectrometer (Bruker BioSpin, Rheinstetten, Germany) and collected with Bruker Xenon software.

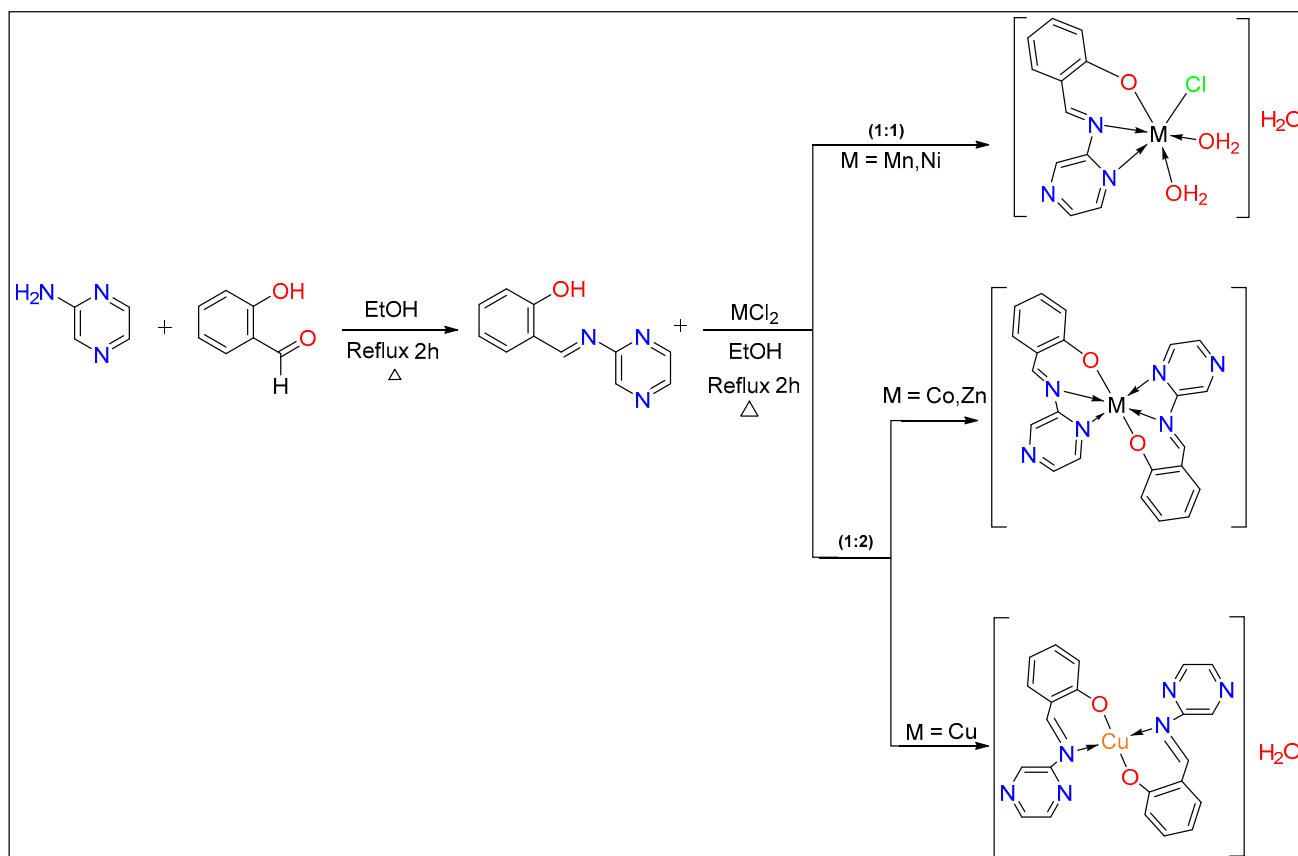
### 2.1. Synthesis of Metal Complexes

The Schiff base ligand that prepared by previous work [12]. Briefly, 2 mmol or 1 mmol of ligand was dissolved in absolute ethanol in 25 mL and adjusted with a drop of NaOH. The solution of 1 mmol of the chloride salts of Co(II), Cu(II), and Zn(II) ions in absolute ethanol was added to the ligand solution and refluxed for 2–3 h. The complex was then filtered, washed with diethyl ether, and dried at room temperature, Scheme 1.

### 2.2. Computational Calculation

Gaussian 09 software package [13] is used to optimize the free Schiff base ligand and its metal complexes. Gauss View software [14] was used to visualize the output files and prepare the figures showing the molecular orbitals (MOs). The DFT method by the hybrid density functional theory, B3LYP, is used with 6-311G for the ligand while the metal complexes were optimized by the LANL2DZ basis set in the gas phase. The obtained vibrational frequencies have indicated the optimized geometry corresponds to valid energy minimum and is scaled by 0.966 and 0.961 factors for 6-31G and LANL2DZ basis set,

respectively. The obtained HOMO and LUMO energies were used to calculate the essential quantum parameters by the following equation: energy gap ( $E_{\text{gap}} = E_{\text{LUMO}} - E_{\text{HOMO}}$ ), absolute electronegativities.



**Scheme 1.** Synthesis of Schiff base and their metal complexes.

( $\chi = -E_{\text{HOMO}} + E_{\text{LUMO}}/2$ ), absolute hardness ( $\eta = E_{\text{LUMO}} - E_{\text{HOMO}}/2$ ), chemical potentials ( $\mu = -\chi$ ), global softness ( $S = 1/2\eta$ ), global electrophilicity ( $\omega = \mu^2/2\eta$ ) [15].

### 2.3. DNA Binding Studies

The DNA-binding abilities of the ligand and its metal complexes were studied by the UV-Vis spectroscopic method. The CT-DNA solution was confirmed to be protein-free by the U.V. absorbance ratio of 1.8 at 260 and 280 nm. All experiments were conducted at a pH value of 7.4 using Tris-HCl buffer and carried out by procedure described earlier [16,17]. The Benassi-Hildebrand equation (Equation (1)) was used to calculate the binding constants ( $K_b$ ) [17].

$$\frac{A^0}{(A - A^0)} = \frac{\epsilon G}{\epsilon(H - G) - \epsilon G} + \frac{\epsilon G}{\epsilon(H - G) - \epsilon G} \times \frac{1}{K_b[\text{DNA}]} \quad (1)$$

[DNA] is the concentration of DNA solution, ( $A^0$ ) is the absorbance of free compounds. ( $A$ ) is the absorbance of the compound in the presence of CT-DNA. ( $\epsilon G$ ) and ( $\epsilon H - G$ ) are their molar absorptivities, ( $K_b$ ) the binding constants. The  $[DNA]/(\epsilon a - \epsilon f)$  versus  $[DNA]$  was plotted against,  $[DNA]$  and the  $K_b$  was calculated from the ratio of intercept to the slope [18,19].

### 2.4. Molecular Docking

Molecular operation environment software (MOE) has been utilized to dock the complexes against protein-receptor; (M14) melanoma cancer (PDB = 2OPZ), (Ovar3) ovarian cancer (PDB = 3W2S), and (HOP-62) (NSCLC) cancer (PDB = 1S9J) which have selected

according to the literature and previous studies [20]. We used the docking protocol that has been described in our previous work [21]. After the crystal structure has been downloaded from the PDB [www.rcsb.org](http://www.rcsb.org) (accessed on 1 July 2021), the water molecules, co-ligand, and metal ions have been removed. The final form was obtained after 3D protonation and the correction process. The MOE site finder generated the active binding sites to create the dummy sites as the binding pocket. The default docking parameters were as follows: triangle matcher for replacing the molecule and London dG for rescoring the docking scores. The DFT optimized structures of the compounds have been used to generate the best five binding poses with flexible molecules rotation. The hydrogen bonds formed between elastase and investigated compound were used to rank the binding affinity and presented as the free binding energy (S, kcal/mol). The higher negative values of the docking scores were presented along with 2D and 3D structures [22].

### 2.5. Anticancer and Toxicological Studies

The cells were supplied by the Egyptian Holding Company for Biological Products and Vaccines (VACSERA) and then kept in the tissue culture unit. The growth of the cells was proceeded in RPMI-1640 medium, supplemented with FBS (10% heat inactivated), penicillin (50 units/mL), and streptomycin (50 mg/mL), and kept in a humidified atmosphere with 5% carbon dioxide [23,24]. The cells were kept as monolayer cultures by serial sub-culturing, obtaining cell culture reagents from Lonza (Basel, Switzerland). The antitumor activities of the complexes were assessed against Ovar-3 (ovarian) NSCLC (lung), and M-14 (Melanoma) cell lines. The sulforhodamine B (SRB) assay method was applied to determine the cytotoxicity, as described in the literature [25]. Exponentially growing cells were gathered using 0.25% Trypsin-EDTA and seeded in 96-well plates at 1000–2000 cells/well in RBMI-1640 supplemented medium. The cells were maintained in the medium for 1 day and then they were incubated for 3 days with various concentrations of the tested complexes. Following 3 days treatments, the cells were fixed with 10% trichloroethanoic acid for 1 h at 4 °C. Wells were stained for 10 min at room temperature with 0.4% SRBC dissolved in 1% acetic acid. The plates were air dried for 24 h and the dye was dissolved in Tris-HCl for 5 min with shaking at 1600 rpm. The optical density (OD) of each well was assessed spectrophotometrically at 564 nm with an ELISA microplate reader (ChroMate-4300, Palm City, FL, USA). The IC<sub>50</sub> values were calculated from a Boltzmann sigmoidal concentration response curve using the nonlinear regression fitting models (Graph Pad, Prism Version 9).

### 2.6. Determination of Acute Toxicity (LD<sub>50</sub>)

The median lethal dose (LD<sub>50</sub>) of the test compounds was determined in mice. A group of male albino mice of five animals (25–30 g) was injected (i.p.) at a specific grade. The percentage of mortality was determined 72 h after injection for each drug under investigation. A prism-9 processed computation of LD<sub>50</sub>

## 3. Results and Discussion

### 3.1. Infrared Analysis

A sharp (C=N) band of the azomethine group was observed 1602 cm<sup>-1</sup> in the free ligand [12]. After complexation, the vibration band of the azomethine group was decreased in intensity and shifted toward a lower frequency about 16–60 cm<sup>-1</sup> in the metal complexes, except the Cu(II) complex that has low intensity band and shifted toward higher frequency about 2 cm<sup>-1</sup>. This shift or disappearance of the peaks support complex formations [26]. The observed sharp band of the pyrazine ring (C=N) in the ligand at 1561 cm<sup>-1</sup> was shifted more than 5 cm<sup>-1</sup> in the metal complexes, except the Cu(II), Table S1. This indicates that the pyrazine ring is involved in coordinating to the metal ions [12]. New broadband in three metal complexes Cu(II), Mn(II) and Ni(II) at 3334, 3315 and 3457 cm<sup>-1</sup> could assign to  $\nu(\text{H}_2\text{O})$  [22].

A new band of  $\nu(\text{M-O})$  band have appeared in the wavenumber range  $522\text{--}575\text{ cm}^{-1}$  and  $\nu(\text{M-N})$  band in range  $424\text{--}444\text{ cm}^{-1}$  [22]. Figure S1 showed the comparison of the IR spectra of the free ligand and the metal complexes.

### $^1\text{H-NMR}$ Spectra for Ligand and Zn(II) Complex

The  $^1\text{H-NMR}$  spectrum of the Schiff base has discussed in detail in our previous work [12]. The signal at 12.38 ppm in the free ligand indicated the presence of phenolic-OH proton has disappeared in the Zn(II) complex spectrum and confirmed the coordination by phenolic oxygen to the zinc ion. In addition, the Schiff base shows another signal at 9.52 ppm which can be ascribed to the azomethine proton ( $-\text{CH}=\text{N}$ ). This signal was shifted to 10.22 ppm after complexing to Zn(II) ion and reveals the involvement of azomethine nitrogen in the coordination of the zinc complex [12]. The  $^1\text{H NMR}$  data for the ligand and Zn(II) are shown in Figure S2 and summarized in Table S2.

### 3.2. Conductance Measurements

The observed molar conductance of the transition metal complexes at range  $\Lambda_M = 26\text{--}58\text{ ohm}^{-1}\text{ cm}^2\text{ mol}^{-1}$  in  $10^{-3}\text{ M}$  DMSO solutions, which suggest the non-electrolytic nature of these compounds.

### 3.3. Molar Ratio

To determine the molar ratio of the metal ion to the ligand molecule. The metal ion standard solution  $1 \times 10^{-4}\text{ M}$  was pipetted into seven volumetric flasks (0, 1, 2, . . . , 6 mL), and a solution of  $1 \times 10^{-4}\text{ M}$  ligand (6, 5, 4, . . . , 0 mL) was added, respectively. All the measurements were carried by a spectroscopic method in a 200–500 nm range. The absorbance measurements were performed by keeping the metal ion concentration constant at  $0.72 \times 10^{-3}\text{ M}$ , while the ligand varied, as shown in Table S3. The absorbance of the sample solution was measured against blank at the maximum wavelength, and the values were then plotted against the ratio of  $[\text{M}]/([\text{M}] + [\text{L}])$  [27]. From the results, we found the inflection was at 0.33 for Co(II) Cu(II) and Zn(II), as shown in Figure 1, while the inflection at 0.5 indicated to 1:1 for Mn(II) and Ni(II) complexes and 1:2 for the other metals.

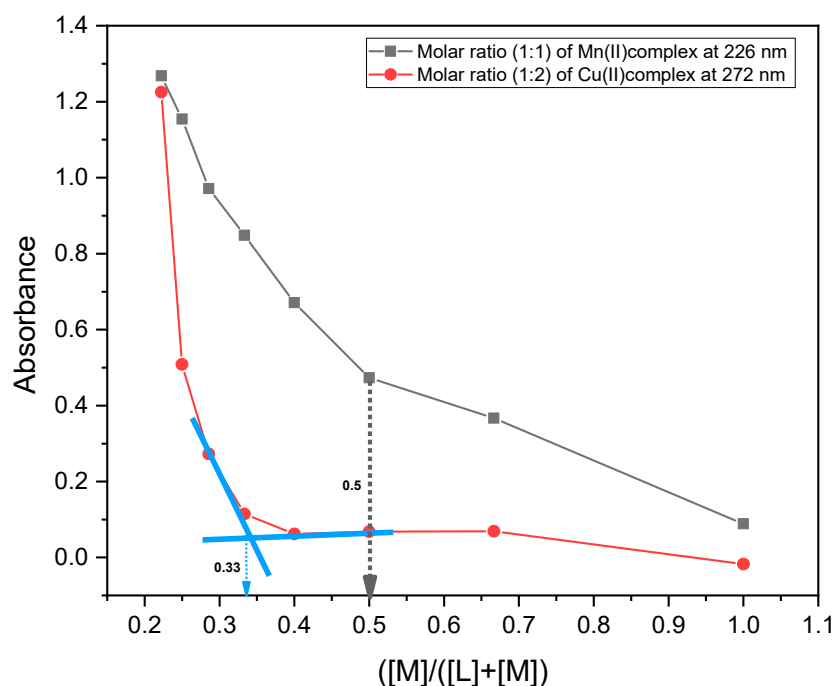


Figure 1. Curves for the molar ratio (1:2) and (1:1).

### 3.4. The Electronic Spectra

Electronic spectral studies for all these complexes were carried out in DMSO at  $10^{-3}$  M concentration. The spectrum of the Schiff base free ligand has observed bands at 264.28, 321.93, and 357.31 nm assigned to  $\pi-\pi^*$  and  $n-\pi^*$  transition, respectively [12]. The metal complexes showed a shift towards lower frequencies of the absorption bands and confirmed the coordination of the ligand to the metallic ions [28]. The electronic spectra of the complexes are shown in Figure S3. Since they are dark-colored complexes, the electronic spectra of d-d transitions are interred with the broad peak of the high excitation coefficient of ligand contribution.

Therefore, they are an expression that is forbidden as the *Laporte rule* of electronic absorptions; this is because the extinction coefficient for these complexes is low compared with the ligand's contribution in the electronic spectra, and it is not easy to see the peaks of these complexes next to the ligand peak.

### 3.5. EPR Spectra for Cu(II) Complex

Electronic paramagnetic resonance spectroscopy is a reliable method to obtain information on the structure of materials with unpaired electrons of complexes [29]. The EPR spectrum of solid Cu(II) complex was obtained at room temperature showed values of  $g_{\parallel} = (2.40)$  and  $g_{\perp} = (2.19)$  as shown in Figure 2. The  $g_{\parallel}$  is greater than the  $g_{\perp}$  value ( $g_{\parallel} > g_{\perp} > 2.0023$ ) and assumed the octahedral, tetrahedral and square planer structure and indicate the ground state of the Cu(II) ion will be  $dx^2 - y^2$  [30]. Further, calculating the value of  $g_{av}$  by this equation  $g_{av} = \frac{(g_{\parallel} + 2g_{\perp})}{3}$  was 2.24 and suggests the covalent character of the metal-ligand bond [17].

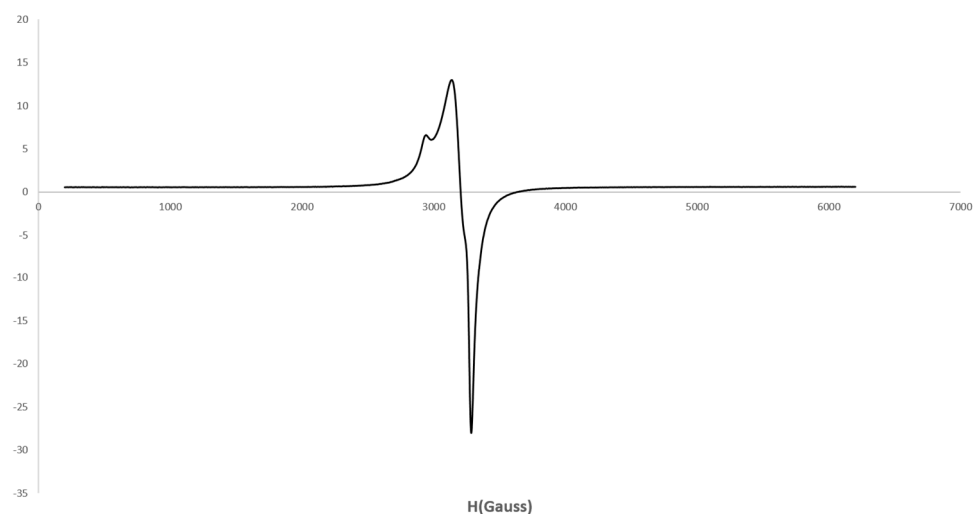


**Figure 2.** EPR spectrum for Cu(II) complex.

### 3.6. Thermal Analysis

Studying the results of the thermal analysis of the metal complexes can expect the number of water molecules, decomposing of the organic molecule in the complexes and metal oxides [31]. The thermogravimetric analysis was measured at room temperature to 800 °C, Figure 3, and the results were summarized in Table S4.

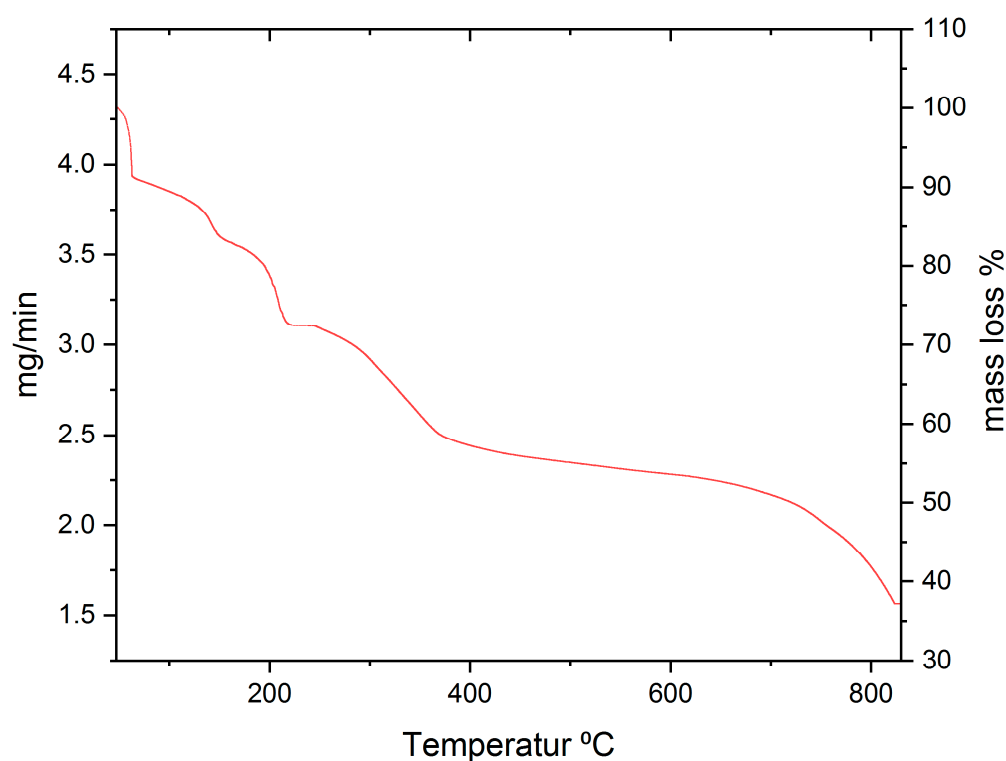


**Figure 3.** TG curve of the Mn(II) complex.

The TG curves of the Mn(II), Ni(II), Cu(II), and Zn(II) complexes showed four decomposition steps while Co(II) complex showed a two-decomposition step; we will discuss them in detail.

- The Mn(II) curve showed four decomposition steps within the temperature ranges of 38.76–821.43 °C, with a mass loss of 47.09% (47.59% calc.). The first step includes the loss of hydrochloric molecular with a mass loss of 10.5% (10.43% calc.), the second step involves losing 3 water molecules with a mass loss of 17.61% (17.79% calc.), the rest of the steps include the loss of organic part as gases with a mass loss of 37.09% (36.66% calc.).
- The Co(II) complex shows two decomposition steps within the temperature ranges of 49.07–473.88 °C, with a mass loss of 84% (84.28% calc.). The first step includes the dehydration of water molecules and loss of the most organic part with a mass loss of 65.5% (66.11% calc.), the second step involved losing the organic interest as a carbon dioxide with a mass loss of 18.5% (18.17% calc.).
- The Ni(II) complex shows four decomposition steps within the temperature ranges of 57.43–800.23 °C, with a mass loss of 64.96% (64.93% calc.). The first step includes the loss of dehydration of 3 water molecules with a mass loss of 14.25% (13.85% calc.); the rest of the steps include the loss of organic part as gases with a mass loss of 50.71% (51.08% calc.).
- The Cu(II) complex shows four decomposition steps within the temperature ranges of 54.60–752.67 °C, with a mass loss of 82.64% (81.73% calc.). The first step includes the loss of water molecules and some of the organic parts as gases with a mass loss of 13.41% (12.84% calc.); the rest of the steps include the loss of organic part as gases with a mass loss of 69.23% (68.79% calc.).
- The Zn(II) complex shows four decomposition steps within the temperature ranges of 55.73–693.79 °C, with a mass loss of 84.54% (85.08% calc.). All four steps involved losing the organic part as gases, with a mass loss of 72.42% (72.5% calc.).

### 3.7. Kinetic Studies

Thermodynamic parameters for the complexes were calculated by employing two methods, the Coast-Redfern integral [32] and the approximation of Horowitz–Metzger [33] methods, to obtain the activation energy ( $E_a$ ). Thermodynamic activation parameters of decomposition processes of the complexes,  $\Delta H$  (enthalpy),  $\Delta S$  (entropy),  $\Delta G$  (Gibbs free energy change of the decomposition), and  $E$  (thermal activation energy) are evaluated graphically, and calculated from the thesis in Equations (2)–(4).

$$\Delta H = E + PV \quad (2)$$

$$\Delta G = \Delta H - T\Delta S \quad (3)$$

$$\Delta S^* = R \ln (Ah/K_B T_s) \quad (4)$$

where  $K_B$  and  $h$  are Boltzmann and Planck's constants, respectively [34,35]. The results are shown in Table S5. Moreover, the general thermal behaviors of the prepared complexes in terms of stability ranges, peak temperatures, and values of kinetic parameters are plotted for Mn(II) complex in Figures 4 and 5.

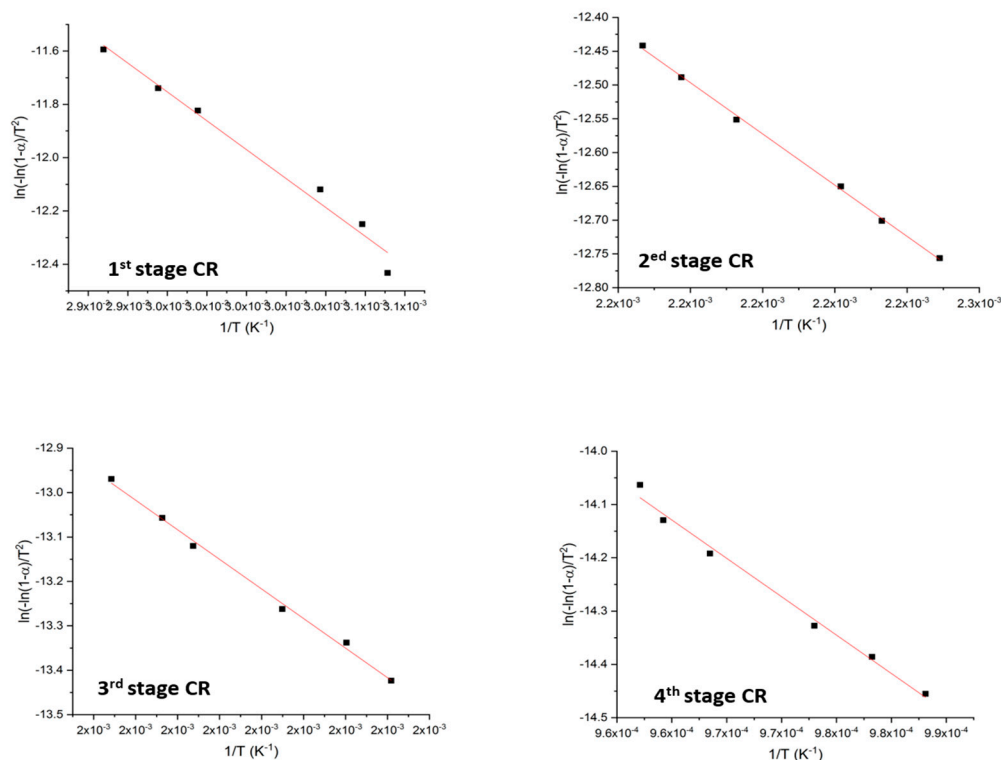
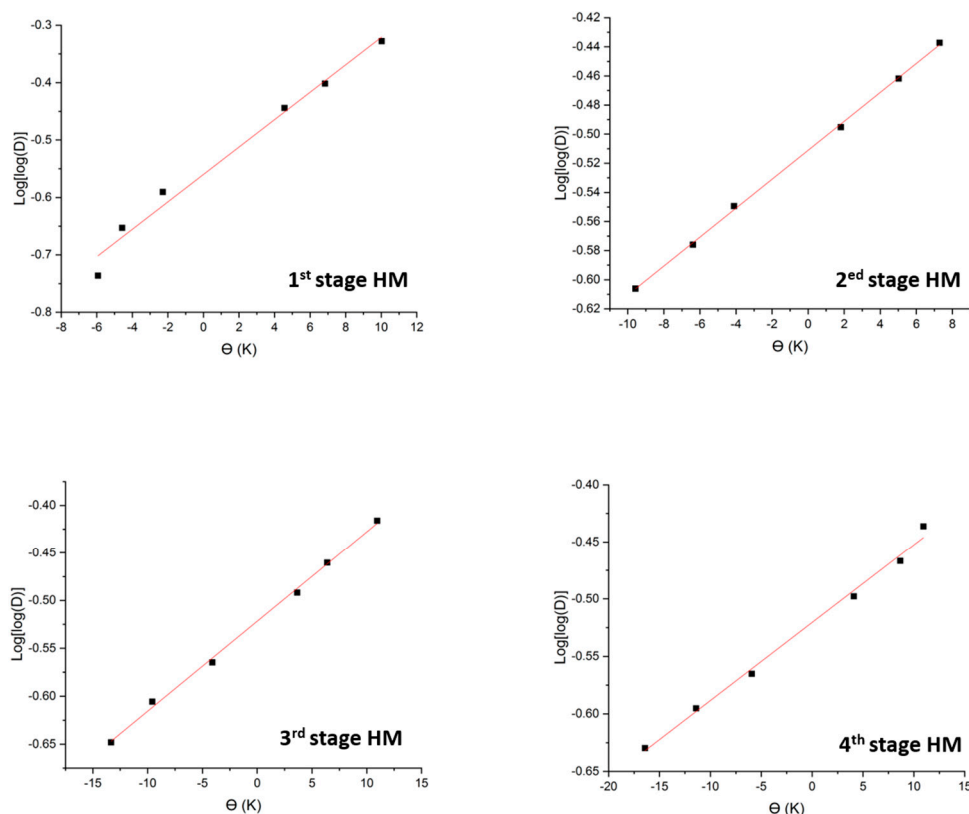


Figure 4. Coast–Redfern of Mn(II) in different stages.

The negative values of  $\Delta S$  indicate pointed to high randomness-degree in non-spontaneous reaction. The positive values of  $\Delta G$  showed the reaction is non-spontaneous towards products and spontaneous towards the reactants and the positive values of  $\Delta H$  means the reaction is endothermic [35,36].



**Figure 5.** Horowitz–Metzger curves of Mn(II) in different stages.

### 3.8. Structural Interpretation

From the above analyses, the suggested structures of these complexes are given in Figure 6 and are matched with previous research. The Schiff base ligand coordinated to metal ions Mn(II), Ni(II) through the N, N, O system [11,37] while Co(II) and Zn(II) [38] was bidentate and bonded through the N, N, O atoms. For Cu(II), the structure is presented in Figure 6.

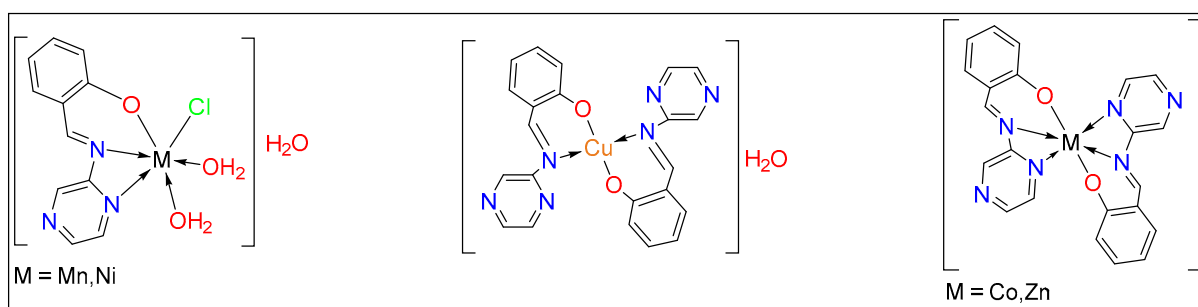


**Figure 6.** Suggested structure for metal complexes.

### 3.9. Calculated Structures

#### 3.9.1. Geometry of the Complexes

We used the obtained results from the spectroscopic analysis (IR, NMR, UV-VIS, and EPR) we proceeded with a computational study to optimize the complex's geometry by the DFT approach. The optimized geometries optimized in the gas-phase of the ligand and its metal (II) complexes were presented with the number and labels of the atoms in Figure 7.

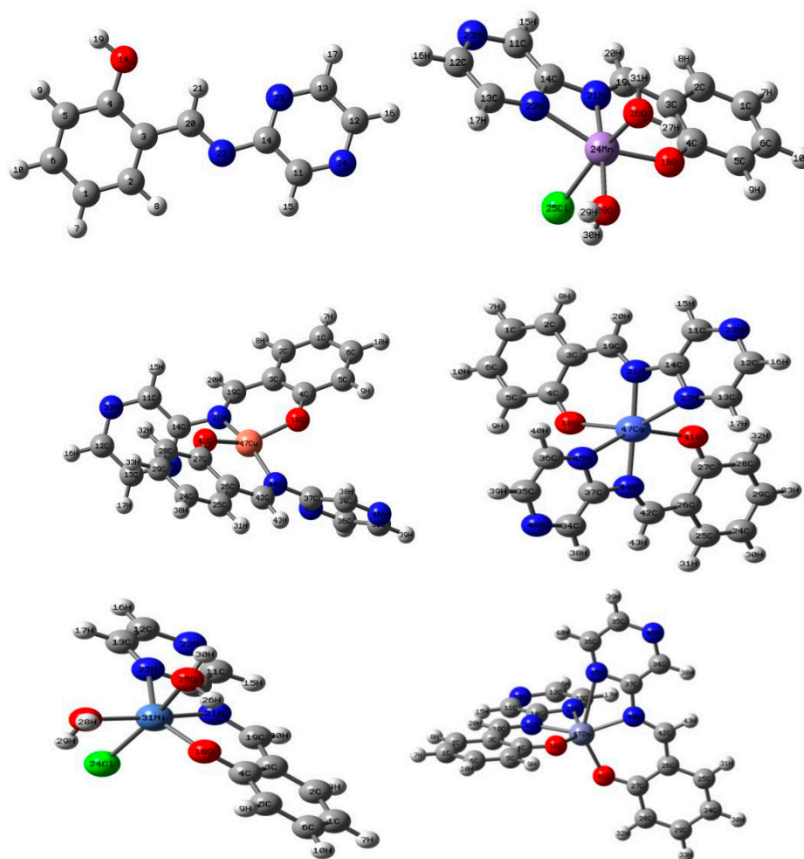


**Figure 7.** Optimized geometry, numbering system, and label for the Schiff base ligand and its complexes using B3LYP/LAND.

A selected geometric parameter around the coordination sphere such as bond length and bond angles for the free ligand and its metal complexes were extracted and tabulated it in Table 1.

The bond length of the free Schiff base showed different characters after bind to the metal ions. The bond length C20–N22 became longer than the free ligand after complexation, whether O18–C4 became shorter by 0.04 and 0.06 Å, respectively. There was a slight change in the C14–N22 and C14–N23 bond lengths around 0.01 or 0.02 Å. In the metal complexes, the primary ligand is coordinated in a bidentate to all metal except Co(II) and Zn(II) that bonded via tridentate from the organic ligand.

The new bonds with the Mn(II) ion, M–O18, and M–N22, were in the reported range of the ionic character of these bonds [39]. Moreover, the other new bonds between the Mn(II) and HO<sub>2</sub> or Cl ion are presented in a covalent bond. Interestingly, all the bonds around Cu(II) ion, M–O, and M–N were ionic bonds with an average length of 1.97 Å. In contrast, the bidentate Ni(II) complexes and tridentate Co(II) and Zn(II) compounds have covalent bonds or medium ionic atmosphere with bond length average = 2 Å.

The importance of bond angles in the coordination complexes comes from the ability to describe the geometric structure of the prepared compounds. Generally, the selected angles around the coordination site in the free ligand, C3–C4–O18 and C3–C20–N22, became bigger after binding to metal ions, while the bond angle between N22–C14–N23 has decreased. The value of the bond angles O18–M–N22, N22–M–N23, H<sub>2</sub>O–M–N22, and H<sub>2</sub>O–M–Cl in the Mn(II) and Ni(II) complexes (Table 1) indicate this complex adopts a distorted octahedral geometry around its respective central metal ion. The deviation from linearity of the bond angles H<sub>2</sub>O–M–O18, H<sub>2</sub>O–M–N23, O18–M–N23, H<sub>2</sub>O–M–N22, and H<sub>2</sub>O–M–Cl confirm this distortion. Similarly, the complexes of Zn(II) and Co(II) showed a distorted octahedral structure. In the Cu(II) complex, the values of the bond angle O18–

M–O41 and N22–M–N44 were 146.07° and 161.30° suggests a highly distorted tetrahedral geometry around the central Cu(II) ions.

**Table 1.** Selected geometric bond lengths and bond angles of the optimized ligand and its complexes using B3LYP/LAND.

Compound	Ligand	Mn	Cu	Co	Ni	Zn
Bond length						
C20–N22	1.29	1.33	1.32	1.33	1.32	1.33
O18–C4	1.39	1.33	1.33	1.32	1.33	1.31
C14–N22	1.40	1.39	1.42	1.39	1.39	1.30
C14–N23	1.36	1.38	1.36	1.37	1.39	1.37
M–O18	-	1.95	1.95	2.03	2.04	2.01
M–N22	-	1.93	1.99	2.05	2.02	2.08
M–N23	-	2.19	-	2.43	2.39	2.67
M–OH <sub>2</sub>	-	2.11	-	-	2.16	-
M–Cl	-	2.44	-	-	2.42	-
Bond angle						
C3–C4–O18	117.18	124.82	123.53	124.50	124.14	123.66
C3–C20–N22	121.1	122.44	127.09	124.08	124.15	125.90
N22–C14–N23	121.5	106.33	116.47	109.84	109.58	111.74
O18–M–N22	-	91.82	92.38	86.84	88.25	88.26
N22–M–N23	-	64.89	-	59.93	60.88	55.99
H <sub>2</sub> O–M–N22	-	100.24	-	-	98.47	-
H <sub>2</sub> O–M–Cl	-	79.98	-	-	80.43	-
H <sub>2</sub> O–M–Cl	-	164.13	-	-	166.48	-
H <sub>2</sub> O–M–N22	-	175.28	-	-	171.29	-
O18–M–N23	-	150.70	-	144.94	146.53	143.84
H <sub>2</sub> O–M–N23	-	114.22	-	-	111.74	-
H <sub>2</sub> O–M–O18	-	89.56	-	-	99.95	-
O18–M–O41	-	-	146.07	107.63	-	107.92
N22–M–N44	-	-	161.30	175.09	-	147.73

### 3.9.2. Ground-State Properties and Global Reactivity Descriptors of the Schiff Base Ligand and Metal Complexes

The frontier orbital energies are important theoretical parameters that contest the highest occupied and the lowest unoccupied molecular orbital energies (HOMO and LUMO, respectively) and the difference between them is called the energy gap ( $E_{\text{HOMO}} - E_{\text{LUMO}} = E_{\text{gap}}$ ) [17]. The calculated energy values for the ligand and its metal complexes were extracted and tabulated with the quantum parameters in Table 2. Figure 8 presents the HOMO and LUMO electron densities calculated by the B3LYP method using the 6-31G basis set for Schiff base and LAND for the metal complexes. For the free ligand,  $E_{\text{gap}}$  was 4.09 eV decreased after complexing with metal ions. The small  $E_{\text{g}}$  indicates the softness and reactivity of the complexes. We can arrange the complexes in the following order, Cu(II) > Mn(II) > Co(II) > Ni(II) > Zn(II). Therefore, the Cu(II) complex presents good reactivity and reveals good toxicity and inhibition activity [40]. Absolute electronegativities ( $\chi$ ), absolute hardness ( $\eta$ ), absolute softness ( $\sigma$ ), chemical potentials ( $\mu$ ), global softness ( $S$ ), global electrophilicity ( $\omega$ ), and additional electronic charge ( $\Delta N_{\text{max}}$ ) are listed in Table 2.

**Table 2.** The calculated quantum chemical parameters of the ligands and their metal complexes.

Compound	HUMO	LUMO	$\Delta E$	$\chi$	$\eta$	$\sigma$	$\mu$	$\sigma$	$S$	$\omega$	$\Delta N_{\text{max}}$
L	−6.44	−2.34	4.09	4.39	2.05	0.49	−4.39	0.49	1.02	4.71	2.14
Ni	−5.80	−2.75	3.06	4.27	1.53	0.65	−4.27	0.76	0.76	2.14	2.79
Co	−5.43	−2.48	2.94	3.96	1.47	0.68	−3.96	0.74	0.74	1.98	2.69
Zn	−5.56	−2.49	3.07	4.03	1.53	0.65	−4.03	0.77	0.77	2.01	2.63
Cu	−5.32	−2.97	2.36	4.14	1.18	0.85	−4.14	0.59	0.59	2.07	3.52
Mn	−5.35	−2.65	2.70	4.00	1.35	0.74	−4.00	0.68	0.68	2.00	2.96

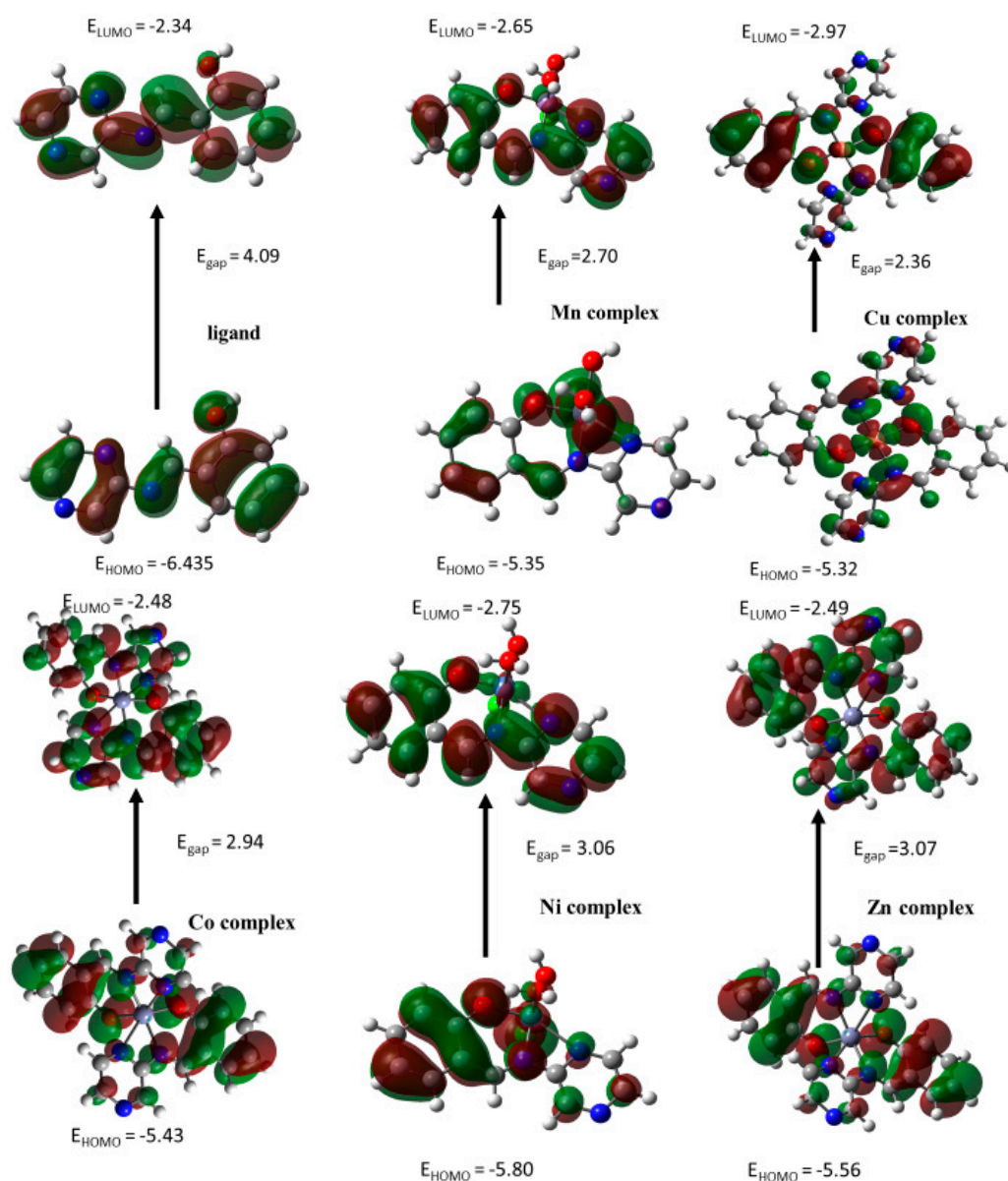


**Figure 8.** The 3D HOMO and LUMO plots of the ligand and the bivalence metal complexes.

### 3.10. DNA-Binding Studies

Electronic absorption titration is one of the easiest methods that helps to predict the type of binding mode of compounds with CT-DNA [41]. In this experiment, the concentration of the metal compounds has been maintained with the variation of the DNA concentration in the range of  $2 \times 10^{-6}$ – $7 \times 10^{-6}$  M.

The free Schiff base ligand spectrum did not show any observed shift after the addition of the DNA nevertheless it showed a reduction in the absorption intensity (hyperchromic), suggesting a weak interaction between the ligand and DNA [42]. The intrinsic binding constant ( $K_b$ ) for the ligand with CT-DNA was  $1 \times 10^6 \text{ M}^{-1}$ .

In general, for the metal complexes, the experiments showed two performances for the metal complexes with increasing CT-DNA concentration, hyperchromic with blue shift or hypochromic with redshift. The complexes of Zn(II) and Mn(II) showed a shift from the  $\lambda_{\text{max}}$  to more than 5 nm. This could indicate the change of the distance between the two helix structures in DNA [41], Figure S4a. The absorption spectra of Ni(II), Cu(II), and Co(II) complexes showed a hypochromic mode with a blue shift which indicated the change in the DNA confirmation or the damage that occurred to the DNA structure [37] Figure S4b.

The binding constant ( $K_b$ ) for the complexes were presented in Table 3. Interestingly, all the complexes gave ( $k_b$ ) values ranging from  $8 \times 10^5$  to  $3.33 \times 10^5$ . Comparing these values with Ru (III) complexes [43], we found that the values were assumed to be intercalation binding types. As observed from Table 3, the Ni(II) complex had the highest binding constant value, followed by the Zn(II) complex.

**Table 3.** Absorption spectral titrations data.

Compounds	$K_b$ ( $M^{-1}$ )	$\lambda_{max}$ Free (nm)	$\lambda_{max}$ Bound (nm)	Type of Chromism
Zn(II)	$5 \times 10^5$	326	321 blue-shift	Hyperchromic
Mn(II)	$3.33 \times 10^5$	300	295 red-shift	Hyperchromic
Ni(II)	$8 \times 10^5$	322	316 blue-shift	Hypochromic
Cu(II)	$3.33 \times 10^5$	294	299 red-shift	Hypochromic
Co(II)	$4 \times 10^5$	326	318 blue-shift	Hypochromic

### 3.11. Molecular Docking

Molecular docking is a computational software regularly used to understanding protein-receptor interaction with complexes [17,44]. The docking process was carried out by simulating the interaction of the Schiff base and their metal complexes with three types of protein-receptors; (M14) melanoma cancer (PDB = 2OPZ), (Ovar3) ovarian cancer (PDB = 3W2S), and (HOP-62) (NSCLC) cancer (PDB = 1S9J) which have selected according to the literature and previous studies [20–45]. The docking study results of the complexes are summarized in Table 4.

**Table 4.** Docking energies for three types of protein with the compounds.

Compounds	S		
	Melanoma Cancer 2OPZ Protein	Ovarian Cancer 3W2S Protein	(NSCLC) Cancer 1S9J Protein
L	−4.82	−5.80	−6.20
Zn(II)	−5.51	−6.55	−7.39
Cu(II)	−5.68	−6.69	−7.29
Ni(II)	−3.79	−3.86	−4.06
Co(II)	−5.50	−6.32	−6.97
Mn(II)	−4.31	−6.13	−5.85

We found that the compounds obtained a high negative value indicating practical bound to the protein. Obviously, Cu(II), Zn(II), and Co(II) complexes gave better results than the ligand. Both Cu(II) and Zn(II) complexes showed the best value compared to the rest of the complexes. We can discuss this binding by way of the following points:

- Cu(II) complex was associated with three hydrogen bonds ( $\pi$ -H) with 2OPZ protein, through the carbon 20 in the complex with the hexagonal ring of the TRP 323, and the five-pointed ring of the TRP 323 amino acid residue, and the benzene ring in the copper complex also associated with the LEU 307 amino acid residue, Table 5 shows the best possible conformation inside the Melanoma cancer 2OPZ protein both the ligand and their metal complexes.
- Cu(II) complex was associated with four hydrogen bonds with 3W2S protein, through the carbon 27 in the complex with the ASP 855 amino acid residue by H-donor bond, nitrogen 19 in the complex with a nitrogen atom in MET 793 amino acid residue by H-acceptor bond, and the benzene ring in the copper complex also associated with the LEU 718 and GLY 796 amino acid residues by  $\pi$ -H bond, are tabulated in Table 5.
- Zn(II) complex was associated with two hydrogen bonds ( $\pi$ -H) with 1S9J protein, through the benzene ring in the complex with the ALA 220 and ASN 221 amino acid residues by  $\pi$ -H bond, are tabulated in Table 5 shows the best possible conformation inside the (NSCLC) cancer 1S9J protein both the ligand and their metal complexes.

**Table 5.** The docking mode of the ligands and their metal complexes, 3D and 2D snapshot showing the hydrophilicity interaction to melanoma cancer target (2OPZ) receptor, ovarian cancer target (3W2S) receptor and (NSCLC) cancer target (1S9J) receptor.

Protein Receptor	Code	3D	2D
melanoma cancer target (2OPZ)	Ligand		
	Zn(II)		
	Cu(II)		

Table 5. Cont.

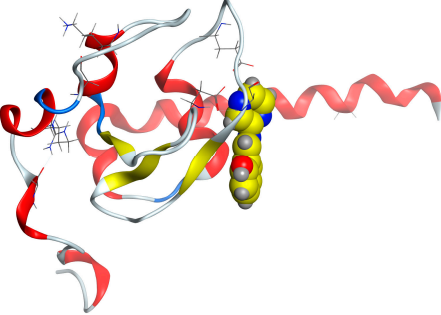
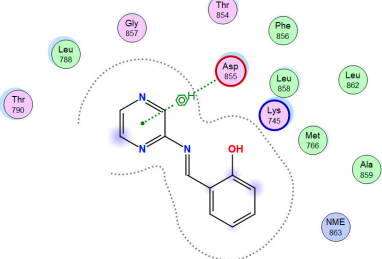
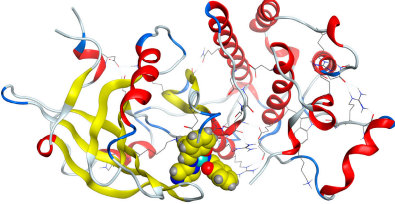
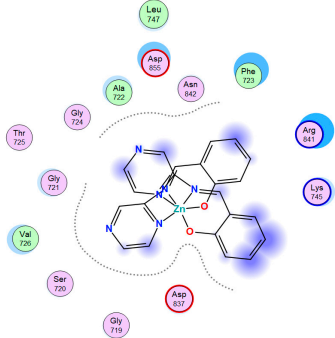
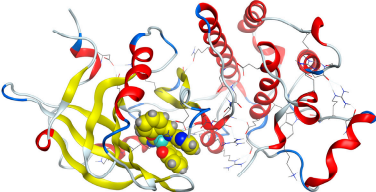
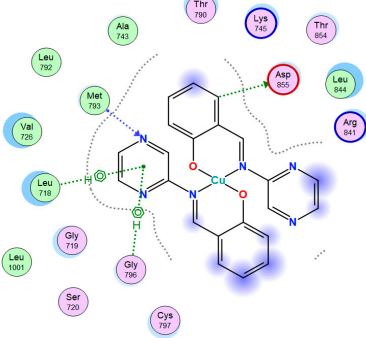
Protein Receptor	Code	3D	2D
ovarian cancer target (3W2S)	Ligand		
	Zn(II)		
	Cu(II)		

Table 5. Cont.

Protein Receptor	Code	3D	2D
(NSCLC) cancer target (1S9J) receptor	Ligand		
	Zn(II)		
	Cu(II)		
		<ul style="list-style-type: none"> <li><span style="color: purple;">○</span> polar</li> <li><span style="color: red;">○</span> acidic</li> <li><span style="color: blue;">○</span> basic</li> <li><span style="color: green;">○</span> greasy</li> <li><span style="border: 1px dashed black; border-radius: 50%; padding: 2px;">○</span> proximity contour</li> <li><span style="color: green;">→</span> sidechain acceptor</li> <li><span style="color: red;">←</span> sidechain donor</li> <li><span style="color: blue;">→</span> backbone acceptor</li> <li><span style="color: red;">←</span> backbone donor</li> <li><span style="color: blue;">●</span> ligand exposure</li> <li><span style="border: 1px solid black; border-radius: 50%; padding: 2px;">○</span> solvent residue</li> <li><span style="border: 1px solid black; border-radius: 50%; padding: 2px;">○</span> metal complex</li> <li><span style="border: 1px dashed black; border-radius: 50%; padding: 2px;">○</span> solvent contact</li> <li><span style="border: 1px dotted black; border-radius: 50%; padding: 2px;">○</span> metal/ion contact</li> <li><span style="border: 1px solid black; border-radius: 50%; padding: 2px;">○</span> receptor exposure</li> <li><span style="border: 1px solid black; border-radius: 50%; padding: 2px;">○</span> arene-arene</li> <li><span style="border: 1px solid black; border-radius: 50%; padding: 2px;">○</span> arene-H</li> <li><span style="border: 1px solid black; border-radius: 50%; padding: 2px;">○</span> arene-cation</li> </ul>	

### 3.12. Anticancer and Toxicological Studies

The Schiff base ligand and their metal complexes were examined against three types of cancer cells. The results are presented in Table 6. The results clarified that metal complexes have better anticancer activities compared to the ligand.

**Table 6.** In vitro anticancer activity of (Ovra3), (M14), and (HOP-62) cancer cell lines.

Code	Types of Cell Cancer								
	Ovar3 (Ovarian)			M14 (Melanoma)			HOP-62 (NSCLC)		
	SD	IC50	LD50	SD	IC50	LD50	SD	IC50	LD50
L	0.05	18.92	430	0.08	14.8	410	0.014	17.45	377
Zn(II)	0.001	9.67	480	0.002	9.78	435	0.001	10.01	370
Cu(II)	0.005	4.17	375	0.005	5.2	388	0.028	11.27	385
Ni(II)	0.018	8.72	389	0.024	9.4	392	0.021	11.1	396
Co(II)	0.001	9.79	480	0.025	8.97	435	0.001	9.45	370
Mn(II)	0.03	5.44	401	0.005	6.33	376	0.035	9	399

Observing the Cu(II) complex has higher activity towards all cancer lines due the pyrazine ring's role which raising the complex's efficiency [46,47]. Hopeful a drug's safety used in vivo can be examined, which means more studies in the laboratory.

The median lethal dose (LD<sub>50</sub>) of the most active anticancer metal complexes for HOP-62 complexes (Zn(II) and Co(II)) in addition these complexes were determined (i.p.) in mice according to reported procedures [48]. The animals got an injection (i.p.) of a specific grade. The results showed that the (LD<sub>50</sub>) of tested compounds were non-toxic at doses up to 370 mg/kg

#### 4. Conclusions

The present work describes the synthesized and characterized of a Schiff base and their metal complexes by analytical and spectroscopic studies. The IR spectra showed a new band at 400 for M–O and 500 M–N indicating that the ligand successfully coordinated to Cu ions through the N, O system and by tridentate system (N, N, O) with other metals ions. The molar ratio data reveal that the ligand to metal ratio is 1:2 for Co(II) Cu(II) and Zn(II), and 1:1 for Mn(II) and Ni(II) complexes. The thermal analysis explained the number of water molecules in the metal complexes. The proposed structures of metal complexes were confirmed by optimizing the geometry of the complexes by the DFT method. The energy gap,  $E_{GAP}$ , for the complexes was lower than that of the ligand, which indicated high activity for the metal complexes. The DNA binding, molecular docking analysis, and anticancer studies suggested that the Schiff base metal complexes were found to be biologically active. The metal complexes showed efficient activity of three cell lines cancer (Ovra3), (M14), and (HOP-62); notably, Cu complex for (HOP-62) showed great results for the safety of the drug used in vivo.

**Supplementary Materials:** The following are available online at <https://www.mdpi.com/article/10.3390/app11199067/s1>, Table S1: comparison between characteristic IR bands experimental and theoretical values, Table S2: major 1H NMR data for ligand and Zn(II) complex, Table S3: experimental data of Cu(II) complex by molar ratio, Table S4: thermoanalytical result of the ligands and their complexes, Table S5: thermodynamic data of thermal decomposition of ligands and its uranyl complexes. Figure S1. IR spectra for ligand and their metal complexes, Figure S2. 1H NMR spectra of Schiff base ligands (a) and Zn(II) complex (b), Figure S3. The electronic spectra of ligand and their complexes, Figure S4. Absorption spectra of (a) Zn(II) complex and (b) the Ni(II) complex in a Tris–HCl buffer upon addition of DNA. The change in the absorbance upon increasing the concentration of DNA is indicated with arrows.

**Author Contributions:** Synthesis and characterizations, H.B.H.; supervision and writing original draft preparation, A.S.B. and M.A.H.; theoretical calculation, review, and editing; A.A.S.; biological studies, interpretations, and English Editing M.H.A. All authors have read and agreed to the published version of the manuscript.

**Funding:** This research received no external funding.

**Data Availability Statement:** All relevant data are within the manuscript and its supporting material.

**Acknowledgments:** We thank King Fahad Medical Research Center for the use of their facilities and support. The simulations in this work were performed at King Abdulaziz University's High-Performance Computing Center (Aziz Supercomputer) (<http://hpc.kau.edu.sa>) (accessed on 20 July 2021), M.H.A expresses her special thanks to Taif University for research support under Project Number TURSP/91, Taif University, Taif, Saudi Arabia.

**Conflicts of Interest:** The authors declare no competing financial interests.

## References

1. Martins, M.A.; Frizzo, C.P.; Moreira, D.N.; Zanatta, N.; Bonacorso, H.G. Ionic liquids in heterocyclic synthesis. *Chem. Rev.* **2008**, *108*, 2015–2050. [[CrossRef](#)]
2. Arora, R.; Sharma, R.; Tazeza, A.; Grewal, A.S.; Saini, B.; Arora, S.; Kaur, R. Design and synthesis of novel 4-aminophenazone Schiff bases by grinding technique as prospective anti-inflammatory agents. *J. Appl. Pharm. Sci.* **2021**, *11*, 48–53.
3. Hameed, A.; Al-Rashida, M.; Uroos, M.; Abid Ali, S.; Khan, K.M. Schiff bases in medicinal chemistry: A patent review (2010–2015). *Expert Opin. Ther. Pat.* **2017**, *27*, 63–79. [[CrossRef](#)]
4. Navale, V.; Shinde, R.; Patil, S.; Vibhute, A.; Zangade, S. Quinazoline based synthesis of some novel heterocyclic Schiff bases. *J. Adv. Chem. Sci.* **2015**, *2*, 201–203.
5. Zhang, B.; Studer, A. Recent advances in the synthesis of nitrogen heterocycles via radical cascade reactions using isonitriles as radical acceptors. *Chem. Soc. Rev.* **2015**, *44*, 3505–3521. [[CrossRef](#)]
6. Ebosie, N.P.; Ogwuegbu, M.O.; Onyedika, G.O.; Onwumere, F.C. Biological and analytical applications of Schiff base metal complexes derived from salicylidene-4-aminoantipyrine and its derivatives: A review. *J. Iran. Chem. Soc.* **2021**, 1–31. [[CrossRef](#)]
7. Malik, M.A.; Dar, O.A.; Gull, P.; Wani, M.Y.; Hashmi, A.A. Heterocyclic Schiff base transition metal complexes in antimicrobial and anticancer chemotherapy. *MedChemComm* **2018**, *9*, 409–436. [[CrossRef](#)]
8. Catalano, A.; Sinicropi, M.S.; Iacopetta, D.; Ceramella, J.; Mariconda, A.; Rosano, C.; Scali, E.; Saturnino, C.; Longo, P. A review on the advancements in the field of metal complexes with schiff bases as antiproliferative agents. *Appl. Sci.* **2021**, *11*, 6027. [[CrossRef](#)]
9. Gaballa, A.S.; Asker, M.S.; Barakat, A.S.; Teleb, S.M. Synthesis, characterization and biological activity of some platinum (II) complexes with Schiff bases derived from salicylaldehyde, 2-furaldehyde and phenylenediamine. *Spectrochim. Acta Part A Mol. Biomol. Spectrosc.* **2007**, *67*, 114–121. [[CrossRef](#)]
10. Ran, X.; Wang, L.; Cao, D.; Lin, Y.; Hao, J. Synthesis, characterization and in vitro biological activity of cobalt (II), copper (II) and zinc (II) Schiff base complexes derived from salicylaldehyde and D, L-selenomethionine. *Appl. Organomet. Chem.* **2011**, *25*, 9–15. [[CrossRef](#)]
11. Sallam, S.; Orabi, A.; Abbas, A. DNA interaction with octahedral and square planar Ni (II) complexes of aspartic-acid Schiff-bases. *J. Mol. Struct.* **2011**, *1006*, 272–281. [[CrossRef](#)]
12. Howsai, H.; Basaleh, A.; Abdellattif, M.; Hassan, W.; Hussien, M. Synthesis, structural investigations, molecular docking and anticancer activity of some novel Schiff bases and their uranyl complexes. *Biomolecules* **2021**, *11*, 1138. [[CrossRef](#)]
13. Frisch, M.; Trucks, G.; Schlegel, H.B.; Scuseria, G.E.; Robb, M.A.; Cheeseman, J.R.; Scalmani, G.; Barone, V.; Mennucci, B.; Petersson, G. *Gaussian 09, Revision d. 01*; Gaussian Inc.: Wallingford, CT, USA, 2009; Volume 201.
14. Dennington, R.; Keith, T.; Millam, J. *GaussView, Version 4.1. 2*; Semichem Inc.: Shawnee Mission, KS, USA, 2007.
15. Sharfalddin, A.; Davaasuren, B.; Emwas, A.-H.; Jaremko, M.; Jaremko, L.; Hussien, M. Single crystal, Hirshfeld surface and theoretical analysis of methyl 4-hydroxybenzoate, a common cosmetic, drug and food preservative—Experiment versus theory. *PLoS ONE* **2020**, *15*, e0239200. [[CrossRef](#)]
16. Sharfalddina, A.A.; Emwas, A.-H.; Jaremko, M.; Hussien, M.A. Transition Metal Complexes of 6-Mercaptopurine; Characterization, DFT Calculation, DNA binding, Molecular Docking, and Anticancer Activity. *Appl. Organomet. Chem.* **2020**, accepted.
17. Sharfalddin, A.A.; Hussien, M.A. Bivalence metal complexes of antithyroid drug carbimazole; synthesis, characterization, computational simulation, and biological studies. *J. Mol. Struct.* **2021**, *1228*, 129725. [[CrossRef](#)]
18. Mashat, K.H.; Babgi, B.A.; Hussien, M.A.; Arshad, M.N.; Abdellattif, M.H. Synthesis, structures, DNA-binding and anticancer activities of some copper (I)-phosphine complexes. *Polyhedron* **2019**, *158*, 164–172. [[CrossRef](#)]
19. Adegoke, O.A.; Ghosh, M.; Jana, A.; Mukherjee, A. Photo-physical investigation of the binding interactions of alumina nanoparticles with calf thymus DNA. *Nucleus* **2019**, *62*, 251–257. [[CrossRef](#)]
20. Jayakumar, J.; Anisetty, S. Molecular dynamics simulations of inhibitor of apoptosis proteins and identification of potential small molecule inhibitors. *Bioorg. Med. Chem. Lett.* **2014**, *24*, 2098–2104. [[CrossRef](#)]
21. Sharfalddin, A.A.; Emwas, A.H.; Jaremko, M.; Hussien, M.A. Synthesis and Theoretical Calculations of Metal–Antibiotic Chelation with Thiamphenicol; In vitro DNA and HSA Binding, Molecular Docking, and Cytotoxic Studies. *New J. Chem.* **2021**, *45*, 9598–9613. [[CrossRef](#)]
22. Hosny, N.M.; Hussien, M.A.; Radwan, F.M.; Nawar, N. Synthesis, spectral characterization and DNA binding of Schiff-base metal complexes derived from 2-amino-3-hydroxypropanoic acid and acetylacetone. *Spectrochim. Acta Part A Mol. Biomol. Spectrosc.* **2014**, *132*, 121–129. [[CrossRef](#)] [[PubMed](#)]
23. Muanza, D.; Kim, B.; Euler, K.; Williams, L. Antibacterial and antifungal activities of nine medicinal plants from Zaire. *Int. J. Pharmacogn.* **1994**, *32*, 337–345. [[CrossRef](#)]

24. Pezzuto, J.M.; Che, C.-T.; McPherson, D.D.; Zhu, J.-P.; Topcu, G.; Erdelmeier, C.A.; Cordell, G.A. DNA as an affinity probe useful in the detection and isolation of biologically active natural products. *J. Nat. Prod.* **1991**, *54*, 1522–1530. [[CrossRef](#)]
25. Skehan, P.; Storeng, R.; Scudiero, D.; Monks, A.; McMahon, J.; Vistica, D.; Warren, J.T.; Bokesch, H.; Kenney, S.; Boyd, M.R. New colorimetric cytotoxicity assay for anticancer-drug screening. *JNCI J. Natl. Cancer Inst.* **1990**, *82*, 1107–1112. [[CrossRef](#)] [[PubMed](#)]
26. Kovacic, J. The C N stretching frequency in the infrared spectra of Schiff's base complexes—I. Copper complexes of salicylidene anilines. *Spectrochim. Acta Part A Mol. Spectrosc.* **1967**, *23*, 183–187. [[CrossRef](#)]
27. Hussien, M.A.; Essa, E.A.; El Gizawy, S.A. Investigation of the effect of formulation additives on telmisartan dissolution rate: Development of oral disintegrating tablets. *Eur. J. Biomed.* **2019**, *6*, 12–20.
28. Mohamed, G.G.; Omar, M.M.; Hindy, A.M. Metal complexes of Schiff bases: Preparation, characterization, and biological activity. *Turk. J. Chem.* **2006**, *30*, 361–382.
29. Sharfalddin, A.A.; Emwas, A.-H.; Jaremko, M.; Hussien, M.A. Complexation of uranyl (UO<sub>2</sub>)<sup>2+</sup> with bidentate ligands: XRD, spectroscopic, computational, and biological studies. *PLoS ONE* **2021**, *16*, e0256186. [[CrossRef](#)]
30. Iqbal, M.S.; Bukhari, I.H.; Arif, M. Preparation, characterization and biological evaluation of copper (II) and zinc (II) complexes with Schiff bases derived from amoxicillin and cephalixin. *Appl. Organomet. Chem.* **2005**, *19*, 864–869. [[CrossRef](#)]
31. Mohamed, G.; Abd El-Wahab, Z. Salisaldehyde-2-aminobenzimidazole schiff base complexes of Fe (III), Co (II), Ni (II), Cu (II), Zn (II) and Cd (II). *J. Therm. Anal. Calorim.* **2003**, *73*, 347–359. [[CrossRef](#)]
32. Coats, A.; Redfern, J. Thermogravimetric analysis. A review. *Analyst* **1963**, *88*, 906–924. [[CrossRef](#)]
33. Siddalingaiah, A.; Naik, S.G. Spectroscopic and thermogravimetric studies on Ni (II), Cu (II) and Zn (II) complexes of di (2, 6-dichlorophenyl) carbazone. *J. Mol. Struct. Theochem* **2002**, *582*, 129–136. [[CrossRef](#)]
34. Canakci, D. Synthesis, Spectroscopic, Thermodynamics and Kinetics Analysis Study of Novel Polymers Containing Various Azo Chromophore. *Sci. Rep.* **2020**, *10*, 477. [[CrossRef](#)]
35. Hosny, N.M.; Hussien, M.A.; Radwan, F.M.; Nawar, N. Synthesis, spectral, thermal and optical properties of Schiff-base complexes derived from 2 (E)-2-(z)-4-hydroxypent-3-en-2-ylideneamino)-5-guanidinopentanoic acid and acetylacetone. *J. Mol. Struct.* **2017**, *1143*, 176–183. [[CrossRef](#)]
36. El-Metwaly, N.; Farghaly, T.A.; Elghalban, M.G. Synthesis, analytical and spectral characterization for new VO (II)-triazole complexes; conformational study beside MOE docking simulation features. *Appl. Organomet. Chem.* **2020**, *34*, e5505. [[CrossRef](#)]
37. Xu, Z.-H.; Chen, F.-J.; Xi, P.-X.; Liu, X.-H.; Zeng, Z.-Z. Synthesis, characterization, and DNA-binding properties of the cobalt (II) and nickel (II) complexes with salicylaldehyde 2-phenylquinoline-4-carboxylhydrazone. *J. Photochem. Photobiol. A Chem.* **2008**, *196*, 77–83. [[CrossRef](#)]
38. Mohamed, G.G.; Omar, M.; Hindy, A.M. Synthesis, characterization and biological activity of some transition metals with Schiff base derived from 2-thiophene carboxaldehyde and aminobenzoic acid. *Spectrochim. Acta Part A Mol. Biomol. Spectrosc.* **2005**, *62*, 1140–1150. [[CrossRef](#)]
39. El-Sonbati, A.; Diab, M.; El-Bindary, A.; Abou-Dobara, M.; Seyam, H. Molecular docking, DNA binding, thermal studies and antimicrobial activities of Schiff base complexes. *J. Mol. Liq.* **2016**, *218*, 434–456. [[CrossRef](#)]
40. Parthasarathi, R.; Subramanian, V.; Roy, D.R.; Chattaraj, P. Electrophilicity index as a possible descriptor of biological activity. *Bioorg. Med. Chem.* **2004**, *12*, 5533–5543. [[CrossRef](#)]
41. Ponya Utthra, P.; Kumaravel, G.; Senthilkumar, R.; Raman, N. Heteroleptic Schiff base complexes containing terpyridine as chemical nucleases and their biological potential: A study of DNA binding and cleaving, antimicrobial and cytotoxic tendencies. *Appl. Organomet. Chem.* **2017**, *31*, e3629. [[CrossRef](#)]
42. Sirajuddin, M.; Ali, S.; Badshah, A. Drug–DNA interactions and their study by UV–Visible, fluorescence spectroscopies and cyclic voltametry. *J. Photochem. Photobiol. B Biol.* **2013**, *124*, 1–19. [[CrossRef](#)]
43. Maheswari, P.U.; Palaniandavar, M. DNA binding and cleavage properties of certain tetrammine ruthenium (II) complexes of modified 1, 10-phenanthrolines—effect of hydrogen-bonding on DNA-binding affinity. *J. Inorg. Biochem.* **2004**, *98*, 219–230. [[CrossRef](#)] [[PubMed](#)]
44. Vijesh, A.; Isloor, A.M.; Telkar, S.; Arulmoli, T.; Fun, H.-K. Molecular docking studies of some new imidazole derivatives for antimicrobial properties. *Arab. J. Chem.* **2013**, *6*, 197–204. [[CrossRef](#)]
45. Sait, K.H.W.; Alam, Q.; Anfinan, N.; Al-Ghamdi, O.; Malik, A.; Noor, R.; Jahan, F.; Tarique, M. Structure-based virtual screening and molecular docking for the identification of potential novel EGFRkinase inhibitors against ovarian cancer. *Bioinformatics* **2019**, *15*, 287. [[CrossRef](#)] [[PubMed](#)]
46. Fabbro, D.; Cowan-Jacob, S.W.; Möbitz, H.; Martiny-Baron, G. Targeting cancer with small-molecular-weight kinase inhibitors. *Kinase Inhib.* **2012**, *795*, 1–34.
47. Frezza, M.; Hindo, S.; Chen, D.; Davenport, A.; Schmitt, S.; Tomco, D.; Ping Dou, Q. Novel metals and metal complexes as platforms for cancer therapy. *Curr. Pharm. Des.* **2010**, *16*, 1813–1825. [[CrossRef](#)] [[PubMed](#)]
48. Abdel-Lattif, M.H.; Kobeasy, M.I.; Abdel-Hafez, S.H. Synthesis, reactions and pharmacological studies of new series of selenolo [2,3-b] tetrahydroquinoline. *Int. J. Basic Appl. Sci.* **2014**, *3*, 433. [[CrossRef](#)]